$A_1t_1(X) + ... + A_nt_n(X)$] where $X = F_{obsd}/F_{max}$.[35] In each case, final difference Fourier synthesis showed no significant residual electron density, and a detailed analysis failed to reveal any systematic errors. All calculations were performed by using the CRYSTALS package on the Chemical Crystallography Laboratory VAX 11/750 computer.

Crystal Data for (*RS*)-[(η^5-C_5H_5)Fe(CO)(PPh_3)CH_2CH_3] (1a): $C_{26}H_{25}FeOP$, M = 440.3, orthorhombic, a = 9.328 (3) Å, b = 17.218 (5) Å, c = 26.810 (7) Å, V = 4306 Å^3, Z = 8, D_{calcd} = 1.36 Mg m^{-3}, μ (Mo Kα) = 7.86 cm^{-1}, space group *Pbca*, relative transmission factors 1.00–1.16, crystal dimensions 0.75 × 0.51 × 0.19 mm, number of reflections [$I > 3\sigma(I)$] 2326, Chebyshev weighting coefficients (A_n) 6.3658, −7.7926, 4.9203, −2.2966, R = 0.035, R_w = 0.037, GOF = 1.07.

Crystal Data for (*RS*)-[(η^5-C_5H_5)Fe(CO)(PPh_3)$CH_2Si(CH_3)_3$] (1e): $C_{28}H_{31}FeOPSi$, M = 498.5, monoclinic, a = 7.941 (3) Å, b = 15.552 (5) Å, c = 20.929 (6) Å, β = 90.69 (2)°, V = 2584.4 Å^3, Z = 4, D_{calcd} = 1.28 Mg m^{-3}, μ (Mo Kα) = 7.06 cm^{-1}, space group $P2_1/c$, relative transmission factors 1.00–1.10, crystal dimensions 0.88 × 0.62 × 0.57 mm, number of reflections [$I > 3\sigma(I)$] 3012, Chebyshev weighting coefficients (A_n) 8.3764, −0.8804, 7.1499, R = 0.032, R_w = 0.039, GOF = 0.97.

(35) Carruthers, J. R.; Watkin, D. J. *Acta Crystallogr., Sect. A.: Cryst. Phys., Diffr., Theor. Gen. Crystallogr.* **1979**, *35*, 698.

Variable Temperature NMR. Spectra were recorded at the higher temperatures in toluene-d_8 or dimethyl sulfoxide-d_6, whilst at lower temperatures dichloromethane-d_2 was the solvent of choice. The coupling constants did not show any significant variation with different solvents, except for complexes **1f** and **1g**.

^{1}H NMR experiments were conducted on a Bruker WH 300 spectrometer at 300.13 MHz. Typically, a sweep width of 3500 Hz was used, and the FID was recorded and processed in 16K blocks of computer memory. Thus, the values obtained for coupling constants are accurate to ±0.2 Hz, whilst the temperature control was accurate to ±1 °C.

^{31}P NMR experiments were conducted on a Bruker AM 250 spectrometer at 101.26 MHz. A sweep width of 10 000 Hz was used, and the FID was recorded and processed in 32K blocks of computer memory. Coupling constants are accurate to ±0.3 Hz and temperature control to ±1 °C.

Acknowledgment. We thank the British Petroleum Company p.l.c. for a Venture Research Award (to M.W.), the SERC for support (to I.M.D.-H. and K.H.S.), Dr. A. E. Derome for conducting differential NOE NMR experiments and for helpful discussions, and Dr. Keith Prout for access to the facilities of the Chemical Crystallography Laboratory, Oxford.

Optical Absorption Spectra of Tetraalkyl Olefin Cation Radicals

Timothy Clark,*[†] Mark F. Teasley,[‡] Stephen F. Nelsen,*[‡] and Hans Wynberg[⊥]

Contribution from the Institut für Organische Chemie der Friedrich-Alexander-Universität, Erlangen-Nürnberg, D-8520 Erlangen, Federal Republic of Germany, S. M. McElvain Laboratories of Organic Chemistry, Department of Chemistry, University of Wisconsin—Madison, Madison, Wisconsin 53706, and Department of Chemistry, University of Groningen, Zernikelaan, Groningen, The Netherlands. *Received February 13, 1987*

Abstract: The cation radicals of five Bredt's rule protected olefins have been investigated by electrochemistry, optical spectroscopy, and MNDO semiempirical molecular orbital calculations. In all cases σ,π^+ transitions involving excitation of an electron from a C–C σ-bonding orbital to the singly occupied π orbital of the olefin cation radical are observed. A simple NCG method for calculating the wavelength of optical absorptions with MNDO, coupled with elementary calculations on the expected intensities, provides a useful tool in interpreting the spectra. Two types of σ,π^+ transitions, where the σ orbital has π^* symmetry, are observed. The first type, a hyperconjugation transition, is found at low energies for the bis-alkylidene cation radicals, where the nodal plane bisects the two alkylidene fragments. In the second type seen for the lowest energy bands of the sesquialkene cation radicals, the nodal plane contains the olefinic carbons and is perpendicular to the π-nodal plane. Through-bond effects are found in the spectra. The sesquihomoadamantene radical cation, 3^+, is kinetically extremely stable.

The current interest in electron-transfer phenomena has led to a rapid improvement in the technique available for the experimental investigation of cation radicals by ESR or optical spectroscopy in matrices[1,2] or in solution.[3,4] The data provided by such experiments are, however, often difficult to interpret or are subject to a variety of explanations. In these cases, molecular orbital calculations can be a valuable tool in resolving difficulties. However, "definitive" calculations can seldom be applied to large organic systems so that lower level ab initio or semiempirical calculations must be tested and adapted to the problems involved. The practical requirement is for computationally efficient but relatively accurate methods to calculate observable parameters reliably for large organic radical ions.

Unfortunately, the experimentally accessible quantities of ESR spectra, hyperfine coupling constants and g values, or optical spectra, λ_{max} and extinction coefficient data, are among those which can be calculated least reliably, even by the highest levels of theory. This paper attempts partly to remedy this situation by reporting experimental and calculated data for a series of large olefin cation radicals and by presenting a simple, effective method for the prediction of λ_{max} for radicals and radical ions.

Olefin cation radicals show hyperconjugation transitions[5] arising from promotion of electrons from σ-bonding orbitals to the π singly occupied molecular orbital (SOMO) of the radical cation. The wavelengths of such σ,π^+ transitions show large and not easily interpretable variations between related cation radicals, so that a method for predicting λ_{max} values is potentially of great value. In this work, we have used the MNDO[6] semiempirical molecular

[†] Institut für Organische Chemie der Friedrich-Alexander-Universität.
[‡] University of Wisconsin—Madison.
[⊥] University of Groningen.

(1) For a review of ESR spectroscopy of cation radicals in matrices, see: Symons, M. C. R. *Chem. Soc. Rev.* **1984**, *13*, 393.
(2) See, for instance; Shida, T.; Hamill, W. H. *J. Am. Chem. Soc.* **1966**, *88*, 5376.
(3) See, for instance: Courtreidge, J. L.; Davies, A. G. *Acc. Chem. Res.* **1987**, *20*, 90.
(4) See, for instance: Asmus, K.-D. *Acc. Chem. Res.* **1979**, *12*, 436. See also ref 17.
(5) Nelsen, S. F.; Teasley, M. F.; Kapp, D. L.; Kessel, C. R.; Grezzo, L. A. *J. Am. Chem. Soc.* **1984**, *106*, 791.
(6) Dewar, M. J. S.; Thiel, W. *J. Am. Chem. Soc.* **1977**, *99*, 4899.
(7) The Dewar Group, AMPAC, Quantum Chemistry Program Exchange, Program No. 506, 1986.

0002-7863/87/1509-5719$01.50/0

Table I. Polycyclic Tetraalkyl Olefin Oxidation and Ionization Potentials and Their Cation Radical Optical Spectra

compd	$E^{\circ\prime}$ (23 °C)/ V[a]	$E^{\circ\prime}$ (−78 °C)/ V[a]	vIP (eV)[b]	cation radical λ_{max}/ nm (ϵ_{min})[c]
1	1.62	1.58	7.84[11]	525 (970), sh 340 (1600)
2	1.68	1.63		450 (750), sh 370 (1300)
3	1.52	1.47		490 (1900), 360 (3500), 265 (5800)
4	1.61	1.56	8.12[12]	sh 440 (810), sh 390 (1300), sh 360 (1700)
5	1.43	1.40	7.90[12]	sh 410 (220), sh 385 (490)

[a] Conditions: 2 mM olefin in 0.1 M tetra-*n*-butylammonium tetrafluoroborate in CH_2Cl_2, at Pt, reported vs. SCE. [b] Gas-phase photoelectron data. [c] Units for ϵ, mol L^{-1} cm^{-1}; sh indicates a shoulder rather than a maximum.

orbital technique with a slightly modified version of the AMPAC[7] program to investigate a series of Bredt's rule protected[8] polycyclic olefin cation radicals and to compare the results with data from experiments in solution.

Results

Electrochemistry and Spectroscopy. Bredt's rule protected olefin cation radicals, in which the C_β–H bonds lie close to the nodal plane of the π-SOMO, are long-lived in solution. In contrast to their unprotected analogues, the radical cations of the Bredt's rule protected tetraalkyl olefins **1**–**5** are persistent enough in solution to allow measurement of their formal oxidation potentials $E^{\circ\prime}$,[8b] which are given in Table I. The intensely green cation radical

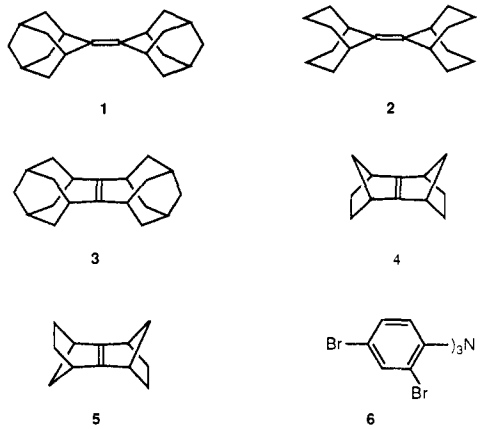

of tris(2,4-dibromophenyl)amine (**6**),[9] first isolated by Schmidt and Steckhan,[10] has $E^{\circ\prime}$ values of 1.68 (23 °C) and 1.66 V (−78 °C) vs. SCE in methylene chloride (0.1 M in *n*-Bu_4NBF_4 as supporting electrolyte). It is therefore a convenient oxidant for generating the cation radicals of **1**–**5**. **2** has the least exothermic electron transfer to $\mathbf{6}^+$ at −78 °C, but an excess of **2** leads to a calculated 96% reduction to **6** under the conditions used to measure the optical spectra. Vertical ionization potentials for **1**,[11] **4**, and **5**[12] are also given in Table I. The ionization potential of **1** (7.84 eV) is slightly lower than that of tetraisopropylethylene (8.13 eV),[11] as would be expected from its increased size. Brown et al.[12] have discussed the reasons for the 0.22-eV difference in vertical ionization potentials between **4** and **5**, but we note that the adiabatic solution oxidation potential of **5** (1.43 eV) is 0.18 eV lower than that of **4** at room temperature.

Optical spectra of $\mathbf{1}^+$–$\mathbf{5}^+$ were obtained in methylene chloride at −70 to −78 °C after oxidation of the olefins with $\mathbf{6}^+SbCl_6^-$. The ϵ_{min} values are significant when comparing band intensities

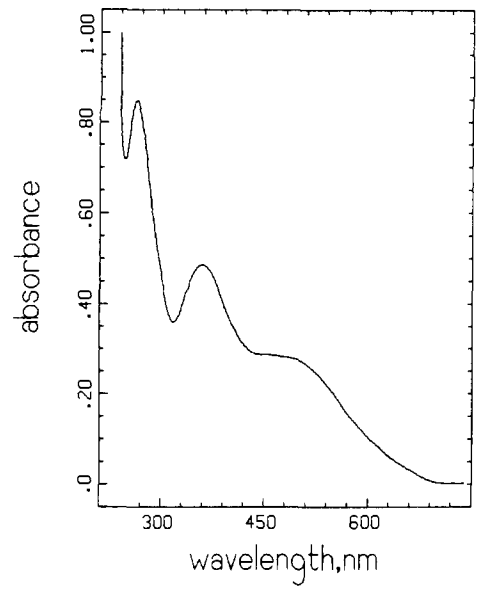

Figure 1. Optical spectrum of electrochemically generated $\mathbf{3}^{\bullet+}$ in 0.1 M TBAP/CH_3CN.

for a given cation but were calculated by ignoring cation decomposition and therefore cannot be compared between cations. They principally reflect the stabilities of the cation radicals. The low wavelength cutoff of spectra under these conditions is about 331 nm because of the intensive absorption of neutral **6** (λ_{max} = 301.5 nm, log ϵ = 4.49). $\mathbf{3}^+$ is far more persistent than the other cation radicals at room temperature so that we were able to record its optical spectrum after electrochemical oxidation in a flow system. This allowed extension of the low wavelength end of the spectrum to 240 nm and revealed a third absorption maximum, as shown in Figure 1. The broadness of the absorption reflects the shortening of the C=C bond on excitation of the cation radicals and possibly the relative ease of twisting about this bond in the ground state.

The ESR spectra for $\mathbf{1}^+$ and $\mathbf{2}^+$ have been reported previously and those of $\mathbf{3}^+$–$\mathbf{5}^+$ have been obtained and simulated.[13] All spectra are consistent with the structure of the olefin used to electrochemically generate the cation radical observed, though a full analysis remains to be completed. The solutions of $\mathbf{1}^+$ and $\mathbf{3}^+$, generated with $\mathbf{6}^+SbCl_6^-$ and examined by optical spectroscopy, proved transferable to the conditions of the ESR experiment and displayed spectra consistent with those above, while those of $\mathbf{2}^+$, $\mathbf{4}^+$, and $\mathbf{5}^+$ could not be successfully transferred. In the case of $\mathbf{1}^+$, its ESR spectrum was seen to decay as the purple color of $\mathbf{1}^+$ faded.[5] The fact that $\mathbf{1}^+$–$\mathbf{5}^+$ display ESR spectra at low temperature and reversible electrochemistry at room temperature argues for the authenticity of their optical spectra.

MNDO Calculations. The prediction of the energies of electronic transitions in cation radicals from the photoelectron spectra is a well-established technique.[14] It is however, of little use for transitions involving promotion from σ orbitals, whose individual energy bands are not usually distinguishable in PE spectra. MNDO has been parametrized[6] to reproduce first-ionization potentials by Koopman's theorem, and it usually also gives useful accuracy for higher ionization potentials (up to about 15 eV).[15] Because almost all observable absorptions for cation radicals involve promotion of an electron from a doubly occupied to the SOMO of the ground state, their energies can be approximated as the difference between the two appropriate Koopman's theorem

(8) (a) Nelsen, S. F.; Kessel, C. R.; Brien, D. J. *J. Am. Chem. Soc.* **1980**, *102*, 702. (b) Nelsen, S. F.; Kessel, C. R. *J. Am. Chem. Soc.* **1979**, *101*, 2503.
(9) Barton, D. H. R.; Haynes, R. K.; Leclerc, G.; Magnus, P. D.; Menzies, I. D. *J. Chem. Soc., Perkin Trans. 1* **1975**, 2055.
(10) Schmidt, W.; Steckhan, E. *Chem. Ber.* **1980**, *113*, 577.
(11) Mollere, P. D.; Houk, K. N., Bomse, D. S.; Morton, T. H. *J. Am. Chem. Soc.* **1976**, *98*, 4732.
(12) Brown, R. S.; Buschek, J. M.; Kopecky, K. R.; Miller, A. J. *J. Org. Chem.* **1983**, *48*, 3692.
(13) (a) Gerson, F; Lopez, J.; Akaba, R.; Nelsen, S. F. *J. Am. Chem. Soc.* **1981**, *103*, 6716. (b) Manuscript on the ESR spectra of $\mathbf{3}^+$–$\mathbf{5}^+$ in preparation with the collaboration of F. Gerson.
(14) (a) Herring, F. G.; McLean, R. A. N. *Inorg. Chem.* **1972**, *11*, 1667. (b) Shida, T.; Nosaka, Y.; Kato, T. *J. Phys. Chem.* **1978**, *82*, 695. (c) Bally, T.; Haselbach, E.; Layiova, Z.; Baertschi, P. *Helv. Chim. Acta* **1978**, *61*, 2488.
(15) See: Clark, T. *A Handbook of Computational Chemistry*; Wiley: New York, 1985; Chapter 4, and references therein.

Table II. MNDO Heats of Formation (kcal/mol^{-1}) and Ionization Potentials (eV)

compd	$\Delta H_f°$	$\Delta H_f°$	Koopman's IP	adiabatic IP	PE vs. IP
1, D_2		174.0		8.34	
1a, D_{2h}	−16.1	176.3	9.42	8.24	7.84[11]
2, D_2		162.1		8.31	
2a, D_{2h}	−29.5	164.1	9.47	8.40	
3, D_{2h}	−16.5	175.7	9.41	8.33	
4, C_{2v}	46.5	234.9	9.13	8.17	8.12[12]
5, C_{2h}	46.2	234.5	9.12	8.17	7.90[12]

ionization potentials for the neutral molecule. The weakness of such an approach, however, is that both vertical ionization potentials in PE spectra and those given by Koopman's theorem in normal MNDO calculatons refer to the geometry of the neutral compound. This problem can be avoided by calculating the Koopman's theorem ionization potentials of the neutral molecule at the geometry of the cation radical (neutral at cation geometry (NCG) calculations). The geometry of the cation radical is calculated with UHF/MNDO[16] and then used for a single-point calculation on the neutral molecule. This calculation then gives a series of Koopman's theorem vertical ionization potentials at the geometry of the ground-state cation radical. Electronic transition energies are simply calculated as the difference between the HOMO energy and that of the orbital from which the electron is promoted. Because the errors in the individual ionization potentials tend to cancel, the predicted transition energies can be very reliable as shown recently for hydrazine cation radicals.[17] Difficulties may arise for transitions involving orbitals centered on elements of the second and higher long periods because MNDO ionization potentials for these elements show systematic errors.[18,19] This can, however, be corrected by a simple technique such as that suggested by Dewar and Healy.[19]

There are, of course, a large number of possible transitions from σ orbitals to the SOMO in $\mathbf{1}^+$–$\mathbf{5}^+$ so that some estimate of the intensity of the transition is very useful in interpreting the spectra. Because only integral intensities can be calculated and because the width of the experimental bands varies so widely, there is little point in trying to reproduce experimental extinction coefficients. However, if a simple zero-differential-overlap approach based on the molecular geometry and the orbital coefficients[20] is used, it becomes clear that the observable transitions are calculated to be one to two orders of magnitude more intense than the others, so that these simple calculated intensities provide a useful interpretive tool. We have therefore modified the AMPAC program to perform NCG calculations on radical systems and to provide calculated wavelengths and intensities. These modifications will be made available for MOPAC.[21]

One further problem involves the structure of tetraalkyl olefin cation radicals. Only the highest level ab initio calculations predict the ethylene cation radical to be twisted, whereas MNDO reproduces[22] the experimentally observed[23] nonpolar structure. MNDO, however, systematically underestimates rotation barriers for planar π-systems[24] and also does not deal well with cation hyperconjugation.[25] We therefore believe that MNDO's good performance for $C_2H_4^+$ may be fortuitous and that it may wrongly predict tetraalkyl olefin cation radicals (whose structures are unknown) to be twisted. This view is reinforced by the fact that MNDO predicts propene cation radical and more highly substituted olefin cation radicals to be highly twisted. The experimental situation is unclear. Propene cation radical was thought to be twisted,[26] but more highly branched olefin cation radicals are planar,[27a] and recent ESR hyperfine coupling constant calculations are consistent with planar structures.[27b] For this reason, we have performed extra calculations on $\mathbf{1a}^+$ and $\mathbf{2a}^+$ in which D_{2h} symmetry was imposed on the system in order to constrain the oxidized double bond to planarity. Table II shows the heats of formation and ionization potentials obtained for the neutral olefin/cation radical systems **1**–**5**. Figure 2 shows some of the more important structural features of the alkenes and their cation radicals.

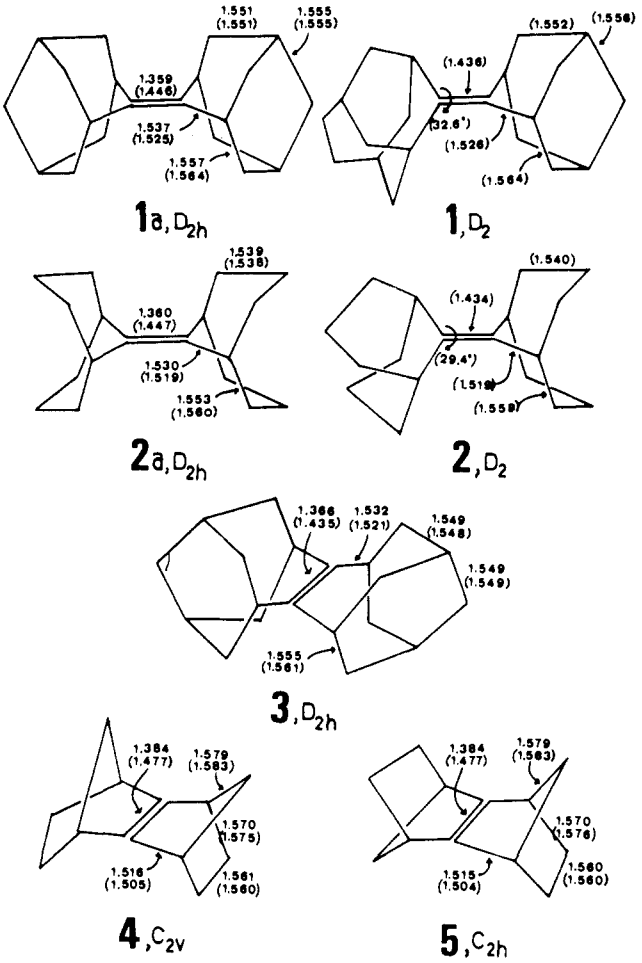

Figure 2. MNDO-calculated geometries (bond lengths in Å) of **1**–**5** and their cation radicals (values in parentheses).

Discussion

Cation Radical Structures. Apart from the lengthening of the double bond from 1.36–1.38 to 1.45–1.48 Å on oxidation, the alkene cation radicals are all calculated to show characteristic hyperconjugative shortening of the vinylic C–C single bonds and lengthening of the allylic hyperconjugative donor bonds α–β to the double bond. MNDO predicts the double bonds in the sesquinorbornenes **4** and **5** to be essentially planar, whereas there is considerable experimental evidence[12] that the syn isomer **4** is significantly bent. This discrepancy probably accounts for the inability of MNDO to reproduce the difference in ionization potentials between **4** and **5**.

(16) (a) Bischof, P. *J. Am. Chem. Soc.* **1976**, *98*, 6844. (b) Dewar, M. J. S.; Olivella, S. *J. Am. Chem. Soc.* **1978**, *100*, 5290. (c) Bischof, P.; Friedrich, G. *J. Comput. Chem.* **1982**, *3*, 486.
(17) Nelsen, S. F.; Blackstock, S. C.; Yumibe, N. P.; Frigo, T. B.; Carpenter, J. E.; Weinhold, F. *J. Am. Chem. Soc.* **1985**, *107*, 143.
(18) Dewar, M. J. S.; McKee, M. L. *J. Comput. Chem.* **1983**, *4*, 84.
(19) Dewar, M. J. S.; Healy, E. F. *J. Comput. Chem.* **1983**, *4*, 542.
(20) Jaffé, H. H.; Orchin, M. *Symmetry, Orbitals, and Spectra*; Wiley: New York, 1970.
(21) Stewart, J. J. P., updated versions of MOPAC will be available from the Quantum Chemistry Program Exchange, Indiana University.
(22) Belville, D. J.; Bauld, N. L. *J. Am. Chem. Soc.* **1982**, *104*, 294.
(23) (a) Merer, A. J.; Schoonveld, L. *J. Chem. Phys.* **1968**, *48*, 522. (b) Koppel, H.; Domcke, W.; Cederbaum, L. S.; von Niesen, W. *J. Chem. Phys.* **1978**, *69*, 4252.
(24) See ref 15 and: Perrin, H.; Berges, J. *THEOCHEM* **1981**, *1*, 299.
(25) See ref 15 and: Dewar, M. J. S.; Thiel, W. *J. Am. Chem. Soc.* **1977**, *99*, 4907.
(26) (a) Shiotani, M.; Nagata, Y.; Sohma, J. *J. Phys. Chem.* **1984**, *88*, 4078. (b) Toriyama, K.; Nunome, K.; Iwasaki, M. *Chem. Phys. Lett.* **1984**, *107*, 86.
(27) (a) Shida, T.; Egawa, Y.; Kubodera, H.; Kato, T. *J. Chem. Phys.* **1980**, *73*, 5963. (b) Clark, T.; Nelsen, S. F., submitted for publication.

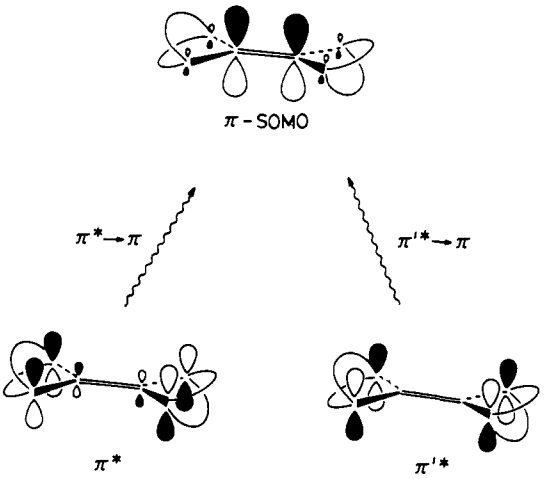

Figure 3. Schematic diagrams of the orbitals involved in σ,π^+ transitions in olefin cation radicals.

$\mathbf{1}^+$ and $\mathbf{2}^+$ are both calculated to be twisted about the central double bond by 32.6° and 29.4°, respectively. The D_{2h}-constrained structures $\mathbf{1a}^+$ and $\mathbf{2a}^+$ are calculated to be 2.3 and 2.0 kcal mol^{-1} less stable than the D_2 cation radicals $\mathbf{1}^+$ and $\mathbf{2}^+$, respectively. The calculated rotational potential surface is therefore very flat so that small energy errors will result in large torsional distortions. The central double bonds in the twisted structures $\mathbf{1}^+$ and $\mathbf{2}^+$ are calculated to be significantly shorter than those in the planar geometries.

σ,π^+ Transitions. Hyperconjugation transitions[28] in alkene cation radicals involve promotion of an electron from doubly occupied σ orbitals that hyperconjugatively stabilize the semicationic centers of the π-SOMO.[5] The most intense of these σ,π^+ transitions are likely to be from the σ orbitals of the same symmetry as the π^* orbital of the double bond. As illustrated in Figure 3, these orbitals interact slightly with the π^* lowest unoccupied molecular orbital (LUMO) to donate electrons to the positively charged centers. Promotion of an electron from such a π^*-type σ orbital into the π-SOMO results in an allowed hyperconjugation transition labeled $\pi^* \rightarrow \pi$ in Figure 3. A second type of allowed transition is that labeled $\pi'^* \rightarrow \pi$ in Figure 3. In this case an electron is promoted from a combination of σ orbitals with a nodal plane containing the olefinic carbons. Strictly speaking, this σ,π^+ transition is not a hyperconjugation transition because the π^*-type σ orbital is symmetry forbidden to interact with the ionized π bond, though it is closely related to the $\pi^* \rightarrow \pi$-type of hyperconjugation transition. Thus hyperconjugation transitions can be seen to be a subset of the larger family of σ,π^+ transitions.

Table III shows the wavelengths and transition moments calculated for $\mathbf{3}^+$, the cation radical for which the best experimental data are available. These results are typical for those calculated for the remaining cation radicals. The two observed absorptions at 490 and 360 nm clearly correspond to the calculated bands at 517.2 and 323.8 nm, respectively. The transition moments of these two excitations are considerably larger than all the others and therefore allow a reliable assignment of the experimental bands. The experimental peak at 265 nm may correspond to the calculated transitions at 271.1 nm or at 224.0 nm. The latter is calculated to be more intense and, as will be shown below, the 224-nm wavelength fits well with the systematic differences between calculated and observed data. On the basis of the data presented in Table III, we have adopted a threshold value of 0.08 for the calculated transition moment and have not considered other excitations. Note that, as expected, there is little quantitative correspondence between the calculated transition moments and ϵ_{min}. Table IV shows all the excitations calculated to have a wavelength longer than 200 nm and a transition moment larger than the 0.08 threshold for the five cation radicals. Also shown are the assignments of the experimentally observed absorptions

(28) See: Olah, G. A.; Pittman, C. U., Jr.; Symons, M. C. R. In *Carbonium Ions*; Olah, G. A., Schleyer, P. v. R., Eds.; Wiley: New York, 1968; also references therein. See also ref 5.

Table III. Calculated Wavelengths and Intensities above 200 nm for $\mathbf{3}^+$

$\lambda_{(calcd)}$[a]	transition moment[b]	λ_{max}(exptl)	ϵ_{min}[c]
205.8	0.0004		
206.6	0		
209.7	0.0295		
222.9	0		
224.0	0.1090	265 (?)	5800
236.3	0		
239.9	0		
243.1	0		
254.3	0.0152		
271.1	0.0889	265 (?)	5800
284.5	0		
291.0	0		
294.6	0		
308.3	0		
323.8	0.3587	360	3500
328.0	0		
339.8	0.0632		
351.3	0		
360.8	0.0587		
371.6	0		
385.6	0.0046		
464.9	0		
470.8	0		
473.3	0.0534		
485.8	0		
508.4	0		
517.2	0.4489	490	1900
559.5	0		

[a] In nm, calculated with MNDO as described in the text. [b] Units: (electronic charge)^2 Å^2. [c] As for Table I.

Table IV. Calculated Optical Absorptions and Assignments for $\mathbf{1}^+$–$\mathbf{5}^+$

cation radical	λ_{MNDO}[a]	transition moment[a]	λ_{max}[b]	λ_{corr}[c]	assignment[d]
$\mathbf{1}^+$, D_2	228	0.09			$^2B_2 \rightarrow {}^2B_1$ ($\pi'^* \rightarrow \pi$)
	296	0.23	340		$^2B_2 \rightarrow {}^2B_3$ ($\pi^* \rightarrow \pi$)
	319	0.11			$^2B_2 \rightarrow {}^2B_3$ ($\sigma \rightarrow \pi$)[e]
	339	0.08			$^2B_2 \rightarrow {}^2B_1$ ($\pi'^* \rightarrow \pi$)
	349	0.08			$^2B_2 \rightarrow {}^2B_1$ ($\pi'^* \rightarrow \pi$)
	459	0.41	525		$^2B_2 \rightarrow {}^2B_3$ ($\pi^* \rightarrow \pi$)
$\mathbf{1a}^+$, D_{2h}	237	0.11		289	$^2B_{2u} \rightarrow {}^2B_{1g}$ ($\pi'^* \rightarrow \pi$)
	312	0.35	340	350	$^2B_{2u} \rightarrow {}^2B_{3g}$ ($\pi^* \rightarrow \pi$)
	361	0.09		389	$^2B_{2u} \rightarrow {}^2B_{1g}$ ($\pi'^* \rightarrow \pi$)
	372	0.11		398	$^2B_{2u} \rightarrow {}^2B_{1g}$ ($\pi'^* \rightarrow \pi$)
	497	0.48	525	497	$^2B_{2u} \rightarrow {}^2B_{3g}$ ($\pi^* \rightarrow \pi$)
	546	0.08		537	$^2B_{2u} \rightarrow {}^2A_g$ ($\sigma \rightarrow \pi$)[e]
$\mathbf{2}^+$, D_2	219	0.12			$^2B_2 \rightarrow {}^2B_1$ ($\pi'^* \rightarrow \pi$)
	311	0.30	370		$^2B_2 \rightarrow {}^2B_3$ ($\pi^* \rightarrow \pi$)
	343	0.14			$^2B_2 \rightarrow {}^2B_1$ ($\pi'^* \rightarrow \pi$)
	414	0.28	450		$^2B_2 \rightarrow {}^2B_3$ ($\pi^* \rightarrow \pi$)
$\mathbf{2a}^+$, D_{2h}	231	0.13		285	$^2B_{2u} \rightarrow {}^2B_{1g}$ ($\pi'^* \rightarrow \pi$)
	334	0.35	370	367	$^2B_{2u} \rightarrow {}^2B_{3g}$ ($\pi^* \rightarrow \pi$)
	375	0.17		400	$^2B_{2u} \rightarrow {}^2B_{1g}$ ($\pi'^* \rightarrow \pi$)
	459	0.28	450	467	$^2B_{2u} \rightarrow {}^2B_{3g}$ ($\pi^* \rightarrow \pi$)
$\mathbf{3}^+$, D_{2h}	224	0.11	265	279	$^2B_{2u} \rightarrow {}^2B_{3g}$ ($\pi^* \rightarrow \pi$)
	271	0.09		317	$^2B_{2u} \rightarrow {}^2B_{1g}$ ($\pi'^* \rightarrow \pi$)
	324	0.36	360	359	$^2B_{2u} \rightarrow {}^2B_{1g}$ ($\pi'^* \rightarrow \pi$)
	517	0.45	490	513	$^2B_{2u} \rightarrow {}^2B_{1g}$ ($\pi'^* \rightarrow \pi$)
$\mathbf{4}^+$, C_{2v}	215	0.28		272	$^2A_1 \rightarrow {}^2B_2$ ($\pi^* \rightarrow \pi$)
				?	
	340	0.32	390	372	$^2A_1 \rightarrow {}^2B_1$ ($\pi'^* \rightarrow \pi$)
			440	?	
$\mathbf{5}^+$, C_{2h}	242	0.22		294	$^2B_1 \rightarrow {}^2A_g$ ($\pi'^* \rightarrow \pi$)
	337	0.29	385	370	$^2B_1 \rightarrow {}^2A_g$ ($\pi'^* \rightarrow \pi$)
			460	?	

[a] As given in Table III. [b] Experimental data from Table I. [c] Calculated λ_{MNDO} corrected according to eq 1. [d] The symbols in brackets give the orbital types from which and to which the electron is excited according to the nomenclature given in Figure 4. [e] Excitation occurs from an in-plane σ orbital.

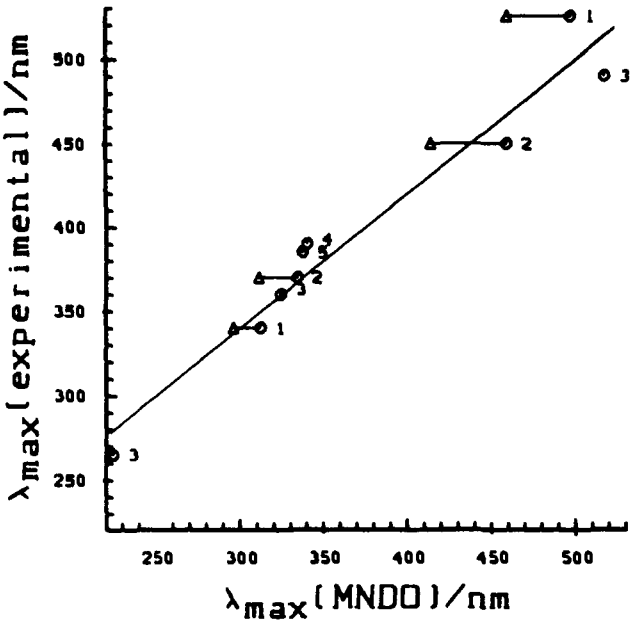

Figure 4. Plot of calculated λ_{MNDO} values against observed λ_{max} data for $1^{\cdot+}$–$5^{\cdot+}$. The circles are plotted with λ_{MNDO} data for $\mathbf{1a}^{\cdot+}$, $\mathbf{2a}^{\cdot+}$, $3^{\cdot+}$, $4^{\cdot+}$, and $5^{\cdot+}$, and the triangles with $1^{\cdot+}$ and $2^{\cdot+}$. The straight line is the least-squares line for the circular points. Assignments are those given in Table IV.

and of the excitations involved. Pleasingly, assignment of the experimental bands to the excitations with the largest calculated transition moments gives a consistent picture of the absorptions involved. The two σ,π^+ bands each observed for 1^+ and 2^+ are due to $\pi^* \rightarrow \pi$-type (hyperconjugation) transitions. In contrast, the two highest σ,π^+ bands for 3^+ and the only assignable ones for 4^+ and 5^+ are suggested to be $\pi'^* \rightarrow \pi$ excitations. This distinction between the bis-alkylidene cation radicals 1^+ and 2^+ and the sesquialkene cation radicals 3^+–5^+ is probably quite general and means that the σ systems determine the nature of the absorptions. The bands at 440 and 360 nm for 4^+ and 460 nm for 5^+ could not be assigned reliably to any calculated excitations into the π-SOMO, the only type which can be treated by the NCG method, at the geometries given in Figure 2. If 4^+ and 5^+ are pyramidalized significantly, then their optical spectra would reflect this in wavelength and intensity of their σ,π^+ transitions. Since MNDO calculates them to be essentially planar and the observed absorptions lie close in energy, a precise study of the geometries of 4^+ and 5^+ would require more information than is afforded by their optical spectra. The ESR spectra of 4^+ and 5^+ suggest that they are pyramidalized, though a quantitative estimate is not yet available. Model calculations do show that the wavelengths of a correlated transition in 5^+ increase with pyramidalization of the olefin carbons, so the unassigned absorptions could be due to such phenomena.

Figure 4 shows a plot of the experimental λ_{max} values against the calculated wavelengths. We had hoped to be able to distinguish between the planar geometries of $\mathbf{1a}^+$ and $\mathbf{2a}^+$ and the twisted structures 1^+ and 2^+ by using such a correlation. Although the correlation coefficient (0.975) including the points calculated for $\mathbf{1a}^+$ and $\mathbf{2a}^+$ is better than that with the twisted forms 1^+ and 2^+ (0.957), the difference is not significant with so few points. However, if the "planar" points are used, the calculated wavelengths (λ_{MNDO}) can be corrected for the systematic deviations by using the equation

$$\lambda_{max}(\text{nm}) = 100.3 + 0.799\ \lambda_{MNDO}(\text{nm}) \ldots \quad (1)$$

Calculated wavelengths corrected according to this equation are given in Table IV. The mean deviation between corrected calculated values and λ_{max} for the nine bands assigned is only 14 nm. The systematic underestimation of λ_{max} below 500 nm by MNDO is linked to the problem semiempirical methods generally encounter with highly branched alkenes.[15] Ionization potentials involving

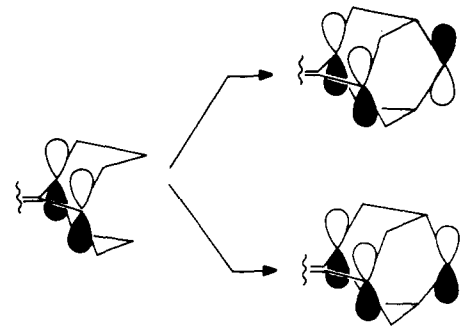

Figure 5. The effect of through-bond conjugation in the π^*-type σ orbitals of $1^{\cdot+}$.

π-orbitals are usually calculated reliably but strain energies, and hence σ energy levels of polycyclic systems present some problems. The λ_{max} values reported here reflect these trends.

Thus, simple NCG–MNDO calculations combined with crude transition moment calculations provide an extremely useful tool for the interpretation and assignment of olefin cation radical optical spectra, and even for their prediction. On the basis of the information gained a more thorough understanding of the factors governing the energies of σ,π^+ transitions is possible. 1^+ and 2^+ illustrate this nicely. The π-SOMO energy levels of the two cations are essentially identical, so that variations in the excitation energy for a given transition mainly reflect changes in the σ orbitals. The 450 nm $\pi^* \rightarrow \pi$ band in 2^+ is red shifted to 525 nm in 1^+, but the related band in 2^+ at 370 nm is blue shifted to 340 nm in 1^+. These effects can be attributed to the extra methylene bridges in 1^+. As shown in Figure 5, these bridges can interact with the appropriate orbitals of the hyperconjugating C_α–C_β bonds via the through-bond effet to destabilize the antibonding combination in 1^+ (and thus shift the $\pi^* \rightarrow \pi$ band to lower energy) and to stabilize the bonding combination. In $2^{\cdot+}$ the methylene orbitals on the central carbons of the trimethylene bridge also perform this function, but not as effectively as the σ_{CC} orbitals in 1^+.

Conclusions

Bredt's rule protected olefins form persistent cation radicals that can be observed in solution by spectroscopy.

Simple MNDO calculations using the NCG approximation to calculate absorption wavelengths and transition moments provide a useful tool for the interpretation of experimental data, especially for compounds containing only C, H, O, and N.

σ,π^+ transitions in olefin cation radicals can be of two principal types and reflect mainly changes in the σ framework, rather than the π bond.

Experimental Section

The low-temperature optical spectra were run on a Cary 18 spectrophotometer modified to accept a Dewar fitted with quartz windows. The Dewar was filled with EtOH cooled initially to −90 °C with liquid N_2. The CH_2Cl_2 solutions of the olefin cation radicals 1^+–5^+ were generated under N_2 or Ar at −78 °C in low-temperature cuvettes with $6^+SbCl_6^-$,[11] then they were suspended in the Dewar to obtain spectra.

The room temperature optical spectrum of 3^+ was run on a Cary 118 spectrophotometer. A 1.0 mM solution of **3** in 0.10 M TBAP/CH_3CN was electrolyzed at a flow rate of 1 mL/min with use of a flow system described elsewhere.[17]

The optical spectra obtained were digitized and replotted with the programs DIGIT and TGRAPH with a Harris/7 computer equipped with a Tektronix Model 4954 graphics tablet and a Calcomp Model 836 digital plotter.

Cyclic voltammetry was performed under the routine conditions given in Table I by following the procedure described elsewhere.[29]

Reference procedures were used to prepare the olefins **1**,[30] **2**,[13a] **4**,[31] and **5**.[32]

(29) Nelsen, S. F.; Kapp, D. L.; Akaba, R.; Evans, D. H. *J. Am. Chem. Soc.* **1986**, *108*, 6853.
(30) Meijer, E. W.; Wynberg, H. *J. Chem. Ed.* **1982**, *59*, 1071.
(31) Paquette, L. A.; Carr, R. V. C. *J. Am. Chem. Soc.* **1980**, *102*, 7553.
(32) (a) Bartlett, P. D.; Roof, A. A. M.; Subramanyan, R.; Winter, W. J. *J. Org. Chem.* **1984**, *49*, 1875. (b) Kopecky, K. R.; Miller, A. J. *Can. J. Chem.* **1984**, *62*, 1840.

Sesquihomoadamantene (3).[33] To a vigorously stirred suspension of 22 g of Na (0.96 g atom) in 300 mL of refluxing xylene was added dropwise 140 g of adamantanone (0.93 mol) in 500 mL of xylene. After 3 h, the reaction was cooled to room temperature and quenched with 50 mL of MeOH and then 200 mL of H_2O. The mixture was acidified with 500 mL of 2 N H_2SO_4 and the precipitate which formed was filtered. The filter cake was washed with H_2O, MeOH, and pentane and then dried to give 124.4 g of 2,2'-dihydroxy-2,2'-biadamantane (88%). Recrystallization from 1:1 hexane-CCl_4 gave an analytical sample (mp 267-269 °C (lit.[33a] mp 267-269 °C; lit.[33c] mp 266-268 °C): ^{1}H NMR ($CDCl_3$, 100 MHz) δ 2.50 (4 H, d, J = 11 Hz), 2.20 (4 H, m), 2.12 (4 H, br s), 1.9-1.4 (20H, m); IR 3620 cm^{-1}; MS, m/e 302(M^+), 150 (100%). Anal. Calcd for $C_{20}H_{30}O_2$: C, 79.42; H, 10.00. Found: C, 79.35; H, 10.0.

To 42 g of H_2SO_4 stirred and chilled in an ice bath was added 15.6 g of 2,2'-dihydroxy-2,2'-biadamantane (51.6 mmol) over a 5-min period. After being stirred for 7 min more, the solution was poured onto 250 g of ice and the precipitate was taken up in Et_2O. The aqueous layer was removed and the Et_2O layer was extracted with H_2O and then saturated aqueous $NaHCO_3$. The Et_2O was dried with $MgSO_4$, filtered, and evaporated to give a quantitative yield of 14.6 g of spiro[adamantane-2,4'-(5'-homoadamantanone)]. Recrystallization from EtOH and then hexane removed the 5% impurity of adamantylidene-adamantane oxide to give 12.5 g of pure ketone (85% mp 178-179 °C, (lit.[33a] mp 176-178 °C, lit.[33] mp 177-178.5 °C)): ^{1}H NMR ($CDCl_3$, 200 MHz) δ 2.72 (1 H, m), 2.54 (3 H, m), 2.2-1.5 (28 H, m); IR 1680 cm^{-1}; MS, m/e 284 (M^+). Anal. Calcd for $C_{20}H_{28}O$: C, 84.45; H, 9.93. Found: C, 84.6; H, 9.95.

To a stirred slurry of 1.82 g of $LiAlH_4$ (47.9 mmol) in 45 mL of Et_2O was added dropwise over an hour 12.5 g of spira[adamantane-2,4'-(5'-homoadamantanone)] (43.9 mmol) in 180 mL of Et_2O. After refluxing 3 h, the reaction was cooled to room temperature and quenched by addition of EtOAc, H_2O, and 100 mL of 2 M HCl. The Et_2O layer was separated and extracted with H_2O and then saturated aqueous $NaHCO_3$. The Et_2O layer was dried with $MgSO_4$, filtered, and evaporate to give 11.7 g of spiro[adamantane-2,4'-(5'-homoadamantanol)] (92%). Recrystallization from 1:2 hexane-CCl_4 gave 10.9 g of alcohol (87%, mp 188-192 °C (lit.[33b] mp 189-192 °C, lit.[33c] mp 191-193 °C)): ^{1}H NMR ($CDCl_3$, 100 MHz) δ 4.12 (1 H, d, J = 5 Hz), 2.6-1.4 (29 H, m); IR 3410 cm^{-1}; MS, m/e 286 (M^+). Anal. Calcd for $C_{20}H_{30}O$: C, 83.85; H, 10.56. Found: C, 83.55; H, 10.5.

To 14 g of P_2O_5 and 40 mL of H_3PO_4 was added 10.9 g of spiro[adamantane-2,4'-(5'-homoadamantanol)] and then the reaction was heated to 140 °C for 2 h. The mixture was cooled and poured onto ice, and the precipitate was taken up in hexane. The aqueous layer was removed, and the hexane layer was extracted with H_2O, saturated aqueous $Na_2S_2O_3$, and brine. After drying with $MgSO_4$, the solution was filtered and evaporated to give 10.0 g of a 3:1 mixture of adamantylidene-adamantane (**1**) and sesquihomoadamantene (**3**). The mixture was dissolved in minimal CCl_4 and 8.9 g of Br_2 in 75 mL of CCl_4 was added dropwise. The resulting precipitate was filtered off, and the filtrate was extracted with saturated aqueous $Na_2S_2O_3$ and then dried with $MgSO_4$. Filtration and evaporation gave crude **3**, which was eluted through Florisil with hexane and evaporated to give 2.51 g (25%). Recrystallization from acetone, followed by sublimation at 0.1 Torr and 130-150 °C, gave 1.60 g of pure **3** (16%, mp 201-203 °C (lit.[33b] mp 199-201 °C, lit.[33c] mp 202-204 °C)): ^{1}H NMR ($CDCl_3$, 200 MHz) δ 2.12 (4 H, m), 1.98 (4 H, m) 1.9-1.6 (20 H, m); IR 1435, 1355, 1070, 1019, 944, 930, 768, and 658 cm^{-1}; MS, m/e 268 (M^+). Anal. Calcd for $C_{20}H_{28}$: C, 89.48; H, 10.52. Found: C, 89.15; H, 10.5.

(33) (a) Wynberg, H.; Boelma, E.; Wieringa, J. H.; Strating, J. *Tetrahedron Lett.* **1970**, 3613. (b) Boelema, E.; Wynberg, H.; Strating, J. *Tetrahedron Lett.* **1971**, 4029. (c) Gill, G. B.; Hands, D. *Tetrahedron Lett.* **1971**, 181.

Acknowledgment. We thank Prof. P. v. R. Schleyer for his interest and the staff of the Regionales Rechenzentrum Erlangen for their cooperation. We thank Professor R. West (Wisconsin) and his group for use of their low-temperature optical spectroscopic equipment. We thank Dr. Nathan Yumibe for his assistance with the electrochemical flow cell. We thank the Petroleum Research Fund, administered by the American Chemical Society, for partial financial support of this work.

Supplementary Material Available: Optical absorption spectra for $\mathbf{1}^{\bullet+}$-$\mathbf{5}^{\bullet+}$ (6 pages). Ordering information is given on any current masthead page.

One-Electron Oxidation Equilibria for Acylated Hydrazines

Stephen F. Nelsen,*[†] Silas C. Blackstock,[†] Peter A. Petillo,[†] Ilana Agmon,[‡] and Menahem Kaftory[‡]

Contribution from the S. M. McElvain Laboratories of Organic Chemistry, Department of Chemistry, University of Wisconsin, Madison, Wisconsin 53706, and Department of Chemistry, Israel Institute of Technology, Technion City, Haifa 32000, Israel. *Received March 11, 1987*

Abstract: Vertical ionization potentials (measured by photoelectron spectroscopy) and formal oxidation potentials (measured by cyclic voltammetry) are reported for trimethylformylhydrazine (**3**), trimethylacetylhydrazine (**4**), 1,2-dimethyl-3-ketopyrazolidine (**5**), 1,1'-bi(2-ketopyrrolidine) (**6**), 2,6-diketo-1,5-diazabicyclo[3.3.0]octane (**7**), 2,5-diketo-1,6-diazabicyclo[4.4.0]decane (**8**), and its 7,10-dimethylene-bridged analogue **9**. X-ray crystal structures are reported for **6** and **7**, ESR spectral data are given for the cation radicals of **7**-**9**, and the NN rotational barrier is reported for **6** (11.4 kcal/mol at -48 °C). The oxidation properties of these acylated hydrazines are compared with those of their tetraalkyl analogues with C=O replaced by CH_2. Large cation relaxation energies (energy differences between vertical and adiabatic cation radicals) are observed even when the nitrogens are planar in the neutral compound. It is concluded that amide resonance is mostly absent in the cation radicals.

Electron removal from tetraalkylhydrazines (R_4N_2) to give their cation radicals (shown for an acyclic example in eq 1) causes a

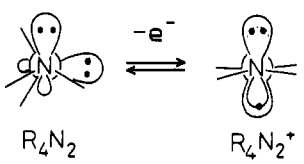

(1)

large geometry change, which dominates the thermodynamics of electron transfer.[1] Neutral R_4N_2 have a substantial preference for pyramidal nitrogen atoms (average bond angle at nitrogen, α(av), ca. 107-111°) and a weak preference for lone pair,lone pair dihedral angle θ near 90°, while the cation radical $R_4N_2^+$ has much less preference for pyramidal nitrogen atoms (p-rich lone-pair hybridization) and a strong preference for coplanar lone pairs (θ = 180 or 0°). Removal of an electron from R_4N_2 may be thought of as generating roughly half a π bond between the

[†] University of Wisconsin.
[‡] Israel Institute of Technology.

(1) (a) Nelsen, S. F. *Acc. Chem. Res.* **1981**, *14*, 131. (b) Nelsen, S. F. *Molecular Structures and Energetics*; Liebman, J. F., Greenberg, A., Eds.; VCH Publishers, Inc.: Deerfield Beach, FL, 1986; Vol. 3, Chapter 1, pp 1-86.

0002-7863/87/1509-5724$01.50/0